Research Article

Investigation of thermal shock resistant in three kinds thermal barrier cerium oxide coating (CeO_2) with MCrAlY intermediate layer

Hossein Ahmadian[1] · Seyed Rahim Kiahoseyni[1]

Received: 17 June 2019 / Accepted: 4 October 2019 / Published online: 16 November 2019

Abstract
The study aimed to compare the thermal shock behavior of three types of thermal barrier coatings (TBC) containing two and five layers. The substrate of the coatings, like as industrial samples, was selected from IN738LC superalloy. The first type was a two-layer TBC produced from CoNiCrAlY and CeO_2 as a bond and top layers, respectively. The second type was a common five-layer TBC with a bond layer of CoNiCrAlY, a top layer of CeO_2 and three intermediate layers composed of three mixing kinds of CeO_2 + CoNiCrAlY. The third type was composed of a top layer of nano-structured CeO_2, and the other four down layers were similar to the second type. To thermal shock test, the samples were kept at 1100 °C for 5 min and quenched in 20–25 °C water. The test was continued until all the samples were destructed. The sample was considered destructed when 20% of the coating surface was detached. To evaluate the microstructure of the samples, SEM and FESEM were used. Finally, the thermal shock lifetime of the five-layer TBC was 1.6 times higher than the two-layer TBC, and by making the top nano-structured layer in five-layer TBC, the lifetime was enhanced approximately 14%.

Keywords Thermal barrier coating (TBC) · Functionally graded materials (FGM) · Plasma spray · Thermal shock · Cerium oxide (CeO_2)

1 Introduction

Increasing high-temperature gas turbines' efficiency and the performance has always been a concern due to the temperature limitations and physical and mechanical stability of the superalloys [1–3]. Thermal barrier coatings are made from the materials with a low heat transfer coefficient to transfer a lower amount of heat to the substrate. In this way, operating temperature of the components and their life span could be increased. In the thermal barrier films, the bond provided favor oxidation resistance for the underlying base metal [4–7].

In new systems, the bond coat is generally one of the MCrAlY (M = Ni and/or Co) coating group. At higher temperatures, such systems developed a thermally grown oxide (TGO) layer in the metal–ceramic interface, which protects the substrate metal surface from oxidation [8, 9]. The top layer provides thermal insulation. This ceramic layer, which is usually made by zirconia (ZrO_2), shows lower thermal conductivity. A stabilized zirconia is used in order to prevent the phase transformation of zirconia and also eliminating the volumetric changes [10–14].

Typically, yttria-stabilized zirconia (YSZ) films are mostly used as thermal barrier. The alumina layer, as a thermally grown oxide (TGO), results high strain energy in this layer, which is due to the thermal unconformity between the TGO and the base metal. The stress created by the excessive growth of TGO is the result of increasing alumina volume due to oxidation aluminum in the bond coat. This strain energy can lead to the TGO distortion, forming and develop cracks, and eventually destroying the thermal barrier coating. Such structures destroyed with the lamination in the coatings [15–19]. Cerium oxide (CeO_2) is one of the lanthanide oxides which are well known for its potential

✉ Hossein Ahmadian, Hosseinahmadian@live.com | [1]Department of Engineering, Damghan Branch, Islamic Azad University, Damghan, Iran.

to oxidation–reduction. Cerium oxide nano-particles are the oxide form of rare cerium element that can imitate dismutase and catalase superoxide activity, because of changing their vacancy of surface oxygen and valence array. So, these nano-particles can be used as scavengers of reactive oxygen species (ROS) in the field of thermal coatings [20–23].

One of the reasons for coating lamination is the differential between the thermal expansion coefficients between layers. One way to reduce this strain is forming the functionally graded material layers (FGM). Functionally graded thermal barrier coatings (FG-TBCs) which have several layers rather than two coats have been proposed to eliminate such problems. In FG-TBC, a gradual change was observed in the layers composition, so this variation makes gradation in the coating layers [function]. This gradual change in the composed of the layers reduces the thermal unconformity strain between layers; this type of coatings has better properties than the dual-layer ones. These properties included higher strength and hardness, greater adhesion of the coating to the substrate and increased the thermal shock resistance. Another method to improve thermal barrier coatings and their quality and life span in different services is adopting nanostructure layers in them. Various researches indicated that in the nano-structured thermal barrier coatings, some properties have been recognized such as strength, hardness, oxidation resistance and wear resistance. The nano-structured films are developed from nano-powders spraying on the surface of the substrate [24–26]. In these nano-particles, one dimension of the powders could reach less than 100 nm. The experimental relationships in the field of physical and mechanical properties indicated a high potential to improve these properties by reducing the particle size [27–29].

So far, extensive researches have been done to compare the thermal shock behavior of TBC and FG-TBC coatings, as well as the conventional thermal barrier coatings versus the nano-structured coatings. For example, in a study, in order to compare the mechanical and microstructural properties of dual-layer TBC coatings in both the conventional and the nano-structured types, the samples of these coatings were applied on the Inconel substrate using the atmospheric plasma spray method. The properties of the coatings were investigated by the adhesion test of coatings, as well as the phase and microstructural analysis of the coating sections. The results indicate the improvement of the nano-structured TBC coating properties compared to the conventional TBC coating [30]. In another study, the comparison of the conventional and the nano-structured dual-layer TBC coatings was performed in terms of thermal cyclic behavior of them. Increments in the life span of the nano-structured coatings compare to the conventional coatings were reported as the results of this investigation [31]. In another research, in order to compare the thermal shock behavior of the dual-layer TBC coatings in both conventional and nano-structured types, the thermal shock test was performed on these specimens in the cycles at 950 °C for 5 min, followed by the rapid quench in water. The results of this test show that the life span of the nano-structured coating is approximately 1.5 times of the conventional coating. To evaluate the quality and the durability of the nano-structured thermal barrier coatings, most researchers have used a nano-structured ceramic layer in the dual-layer TBC thermal insulation coatings [32, 33].

In this study, the nano-structured coatings in the top ceramic layer of five-layer FG-TBC thermal insulation coating were used to investigate the quality and the life span of the nano-structured thermal barrier coatings. In order to analyze the properties of the nanostructure layer in this coating, in addition to the five-layer nanostructure thermal barrier coating (FG-TBC), the five-layer conventional thermal barrier coating and the dual-layer conventional thermal barrier coating (TBC) were evaluated. By performing a thermal shock test on these three types of the thermal barrier coatings, it is possible to compare the fracture strength of these coatings in the shock test.

2 Experimental activities

The first coating type (A) was a two-layer TBC. The second type (B) was a common five-layer TBC (FG-TBC), and the third one (C) was a five-layer TBC (FG-TBC) containing a top nano-structured ceramic layer (the schematics of the two coatings are illustrated in Fig. 1). In Fig. 1, the composition and thickness of each layer of the three coatings were determined. Coating A is the most current TBC used in various industries. In coating B and C, the composition of the intermediate layers was a mixture of the composition of top and bond layers that the composition of each layer was shown in Fig. 1. In this research, the total thickness of coating layers in all the samples was the same and was approximately 450 µm. The composition of substrates was selected from IN738LC superalloy, widely used in industries and engineering fields. The properties of the superalloy are shown in Table 1. The substrate was cut in disks with a diameter of 20 mm and a thickness of 14 mm. In the samples, CeO_2 powders (202975, Sigma, USA) with the purity of 99.99% and CeO_2 nano-powders (544841, Sigma, USA) with the dimensions of lower than 25 nm were used.

To coat the bond layer, the metal powder of CoNiCrAlY (415.006, Amperit, Sweden) with the composition of $Co_{32}Ni_{21}Cr_8Al_{0.5}Y$ was applied. In this research, the coating of the samples was done via an atmospheric plasma spray (APS) method, and the applied parameters of coating of each layer were indicated in Table 2. In addition,

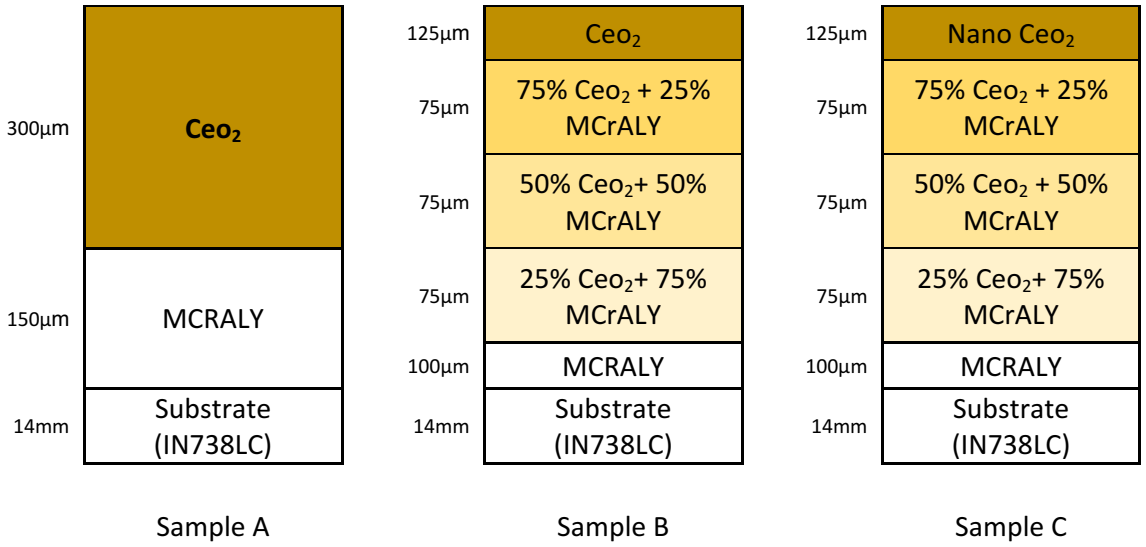

Fig. 1 Schematic of designed coatings

Table 1 Properties of IN738LC superalloy

Composition	Si	Nb	Zr	B	C	Ti	Al	Mo	Co	Cr	Ni
Proportion by mass (%)	0.5	1.5	0.1	0.012	0.05	0.8	5.3	4.2	1	12.5	74

Table 2 Applied parameters of plasma spraying for the coating of each layer

Parameters	CoNiCrAlY	25%–75%	50%–50%	25%–75%	CeO_2	Nano CeO_2
Gun type	MB3	MB3	MB3	MB3	MB3	MB3
Argon flow rate (SCFH)	85	85	85	80	80	80
Hydrogen gas flow rate (SCFH)	15	15	15	15	15	15
Argon powder carrier gas	30	30	30	30	30	30
Spray distance (cm)	12	12	10	8	8	8
Current (A)	450	450	470	480	500	450
Voltage (V)	50	50	55	55	55	55
Powder feed rate (Lbs/h)	10	10	15	15	15	15

after coating each layer, its thickness was investigated via thickness meter.

To thermal shock test, for each coating type, triplicate samples were produced, and each sample was kept in a furnace at 1100 °C for 5 min and then rapidly quenched in water at 20–25 °C. After bringing out and drying the samples, they were put again in the furnace, and the steps mentioned above were repeated. The repeating cycles were continued until all the samples were destructed. The fracture cycle number was reported when the sample was destroyed. The sample was considered destructed when it delaminated, and 20% of its coating surface was destroyed. After destructing the sample, the test was stopped, and the number of applied thermal shock cycles was reported as a fracture cycle number. After destroying all the samples based on the aforementioned criterion and recording their fracture cycle numbers, the test was accomplished.

3 Results and discussion

To evaluate the microstructure of applied coats, before the thermal shock test, the cross section of each sample was prepared and investigated via a scanning electron microscopy (SEM). Furthermore, the surface micrographs of the samples were assessed via a field-emission scanning electron microscopy (FESEM). In Fig. 2, the micrographs of cross sections and surfaces of the three coats are shown. In the cross-sectioned micrographs, the different layers of the coating with the powder mixture of each layer, based on the composition mentioned above in Fig. 1, were

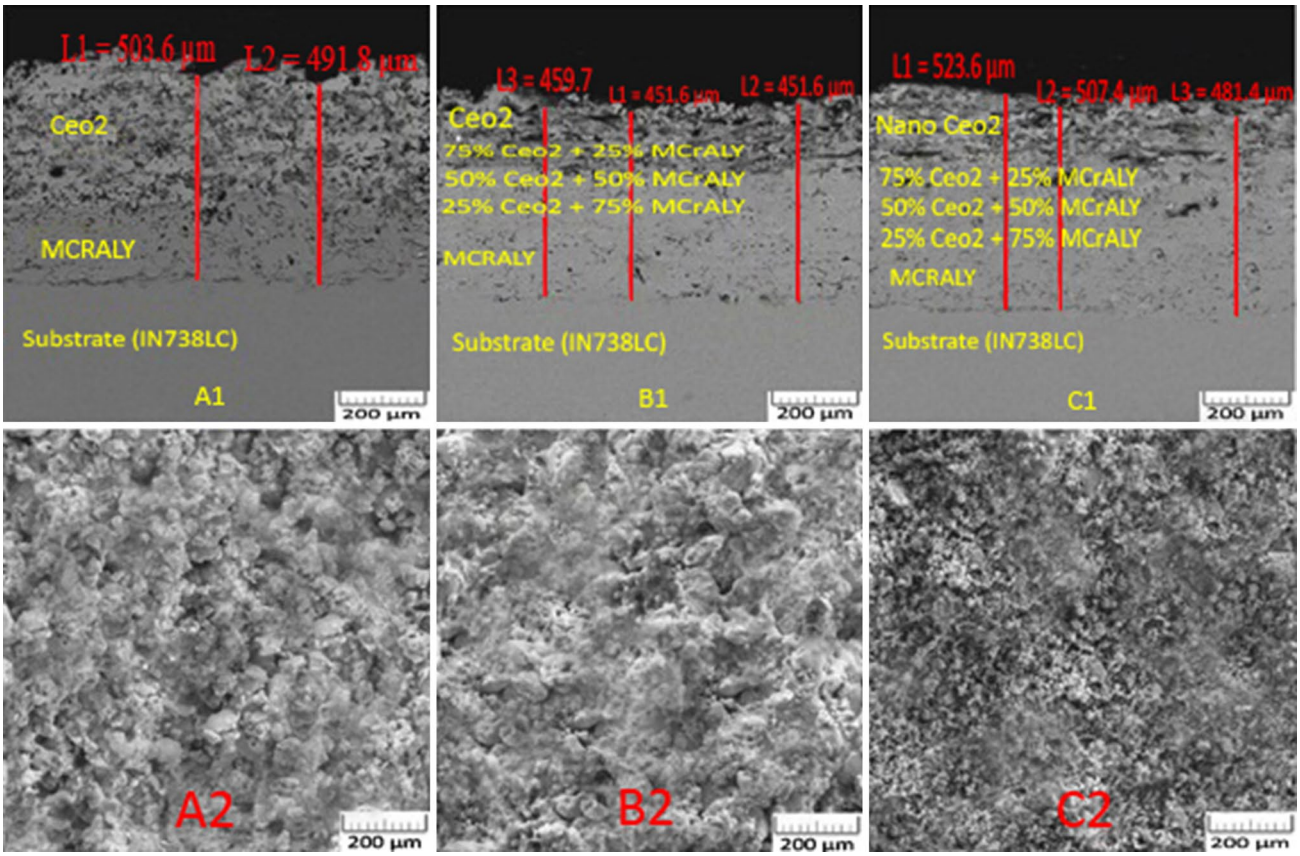

Fig. 2 A1, B1 and C1 are the cross section of sample A, B and C, respectively, and A2, B2 and C2 are the coated surface of sample A, B and C, respectively

illustrated. Moreover, the total thickness of the coating layers was determined.

In sample B and C, the presence of the intermediate layers created a moderate concentration incline between the top and bond layers. Through the layers, although it cannot be possible to determine the interface of the layers clearly, the zone of each layer can approximately be distinguished. As it can be seen in the FESEM micrographs of the coating surfaces, the coated surface of sample A and B are similar, because of the similarity in their top layers, but the coated surface of sample C is different compared to the others, because of its top nano-structured ceramic layer.

In the plasma sprayed nano-structured TBCs, their coated surface consisted of the matrix of re-solidified complete-melted particles and the nano-domains of non-melted particles. The structures are observable in micrograph C2. For the affirmation of the nano-particle's presence in the coated surface, the magnification of FESEM was increased until the dimensions of the nano-particles can be distinguishable. In Fig. 3, FESEM micrograph of the coated surface of sample C is shown at 75 k×

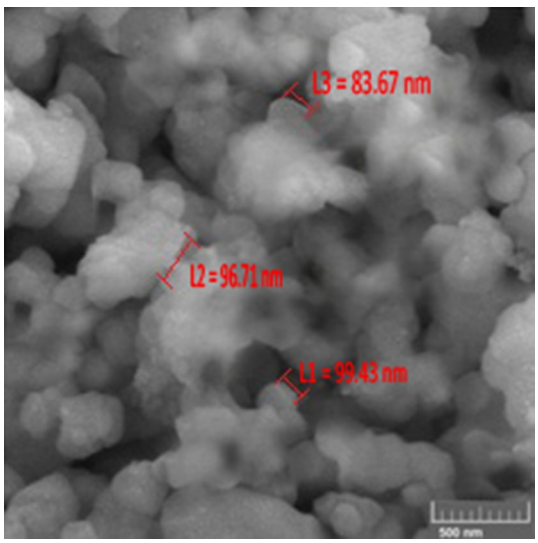

Fig. 3 FESEM micrograph of CeO_2 nano-particles in the coated surface of sample C at 75 k× magnification

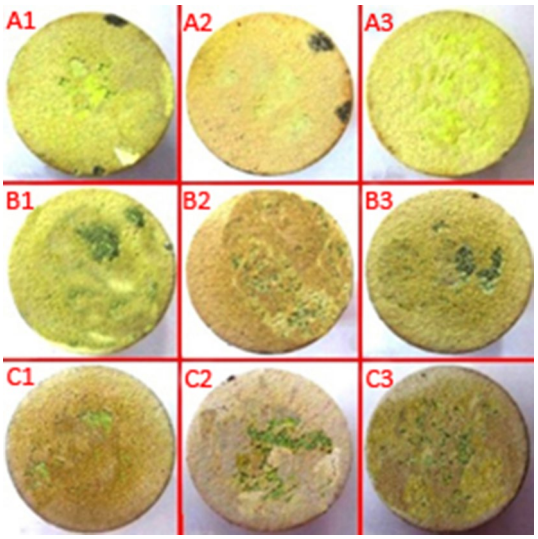

Fig. 4 Picture of the surface of the specimens disintegrating after the heat shock cycles

Table 3 Fracture cycle number of the samples determined by the thermal shock test

	Types of coating A	Types of coating B	Types of coating C
Sample 1	259	403	483
Sample 2	270	414	454
Sample 3	265	426	477
Average samples	265	414	471

magnification. In this micrograph, the dimension of including nano-particles, CeO_2 nano-particles, was determined.

The fracture cycle number of sample A determined by the thermal shock test was 259, 270 and 265 cycles. In sample B, their fracture cycle number was increased because of the presence of functionally graded material in the intermediate layers. Their fracture cycle number was 403, 414 and 426 cycles. In sample C, the presence of the nano-structured CeO_2 top layer increased the fracture cycle number up to 483, 454 and 477 cycles. In Fig. 4, the scaling and surface degradation of the samples of these three types of coatings according to the desired failure criterion are shown after the reported heat shock cycles.

In Table 3, the fracture cycle number of the three coats determined by the thermal shock test was reported. The fracture cycle number of all the samples is shown in Fig. 5 in the form of linear and columnar diagrams.

The average fracture cycle number of sample A, B and C, as shown in Fig. 6, was 265, 414 and 471 cycles, respectively. According to the obtained results, by changing the structure of two-layer TBC to five-layer FG-TBC, the fracture cycle number determined by the thermal shock test was increased and in consequence, the lifetime of the coating was enhanced. So, to improve the lifetime of two-layer TBC, FG-TBC can be proposed, because by increasing the layer number of the coating, it can be possible simultaneously to improve binding of the coating layers to the substrate, increase the lifetime of the coating and enhance its quality. In addition, the creating of the nano-structured FG-TBC caused an increase in the fracture cycle number determined by the thermal shock test and the lifetime of the coating. The event originated from the modification of the coating structure to nano-scale that decreased the porosity of the coated surface. So, oxygen diffusion to the lower layers was prevented and destruction of the

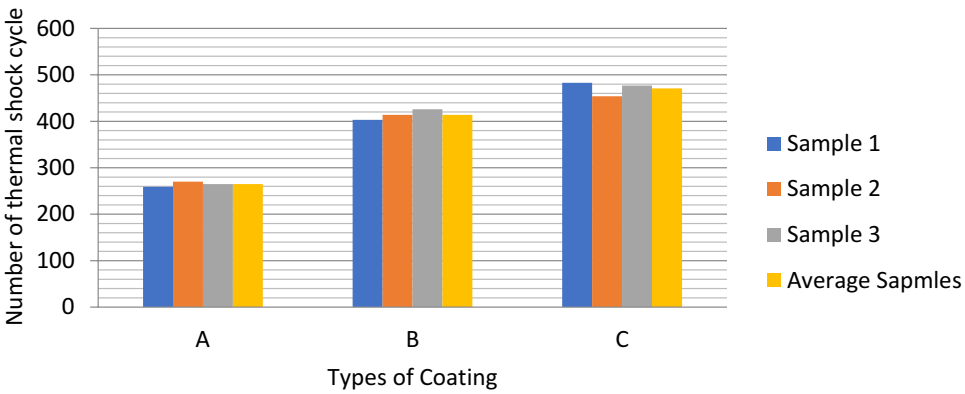

Fig. 5 Columnar diagram of the fracture cycle number of the samples determined by the thermal shock test

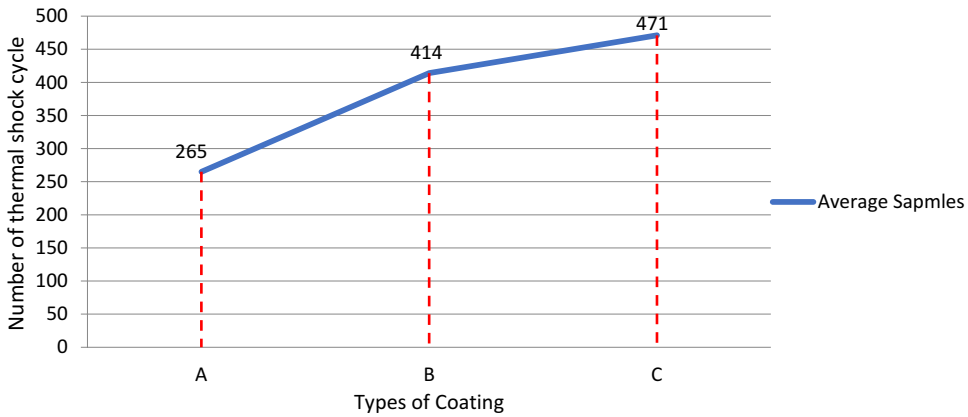

Fig. 6 Linear diagram of the fracture cycle number of the samples determined by the thermal shock test

layers was delayed. At the end of the thermal shock test and destruction of all the samples based on the criterion mentioned above, from each coating type, a sample was selected, mounted and cut to evaluate its cross section by an SEM. In Fig. 7, SEM micrographs of the cross-sectioned sample A1, B2 and C3 after applying the thermal shock test are shown. In micrograph A1, crack formation and growth through the coating layers and their destruction are observable. Most of the destruction happened in the ceramic layer. In the two-layer TBC, because of the high thickness of CeO_2 layer (that was about 2/3 of the total coating thickness), cracks grew in all the thickness of the ceramic layer and approached to the metal substrate. Crack growth was also observed in the ceramic layer of sample B2; however, its growth and destruction effect appeared in the more defined zone because of the reduction in the ceramic layer thickness. In micrograph C3, the crack growth and its destruction effect were only observed in the ceramic layer, but in the lower scale compared to sample B2. The stress originated from continuously applied thermal cycles can cause crack nucleation and growth in the coat. By joining the grown cracks and continuing its growth in the parallel direction of the interface, delamination appeared in the coat surface. Hence, the stresses resulted from noncompliant thermal expansion coefficients were the main reason of TBC delamination.

In the common plasma sprayed ceramic coating, the crack grew through the inter-splat boundaries. However, in the nano-structured coating, because the nano-domains pinned the inter-splat boundaries, the crack growth was prevented by the domains, and its growth direction deviated. So, it was expected that the nano-structured TBC compared the common one can tolerate more thermal cycles. The results obtained from this study also confirmed that the creation of the top nano-structured ceramic layer in FG-TBC enhanced the thermal shock resistance of the coating.

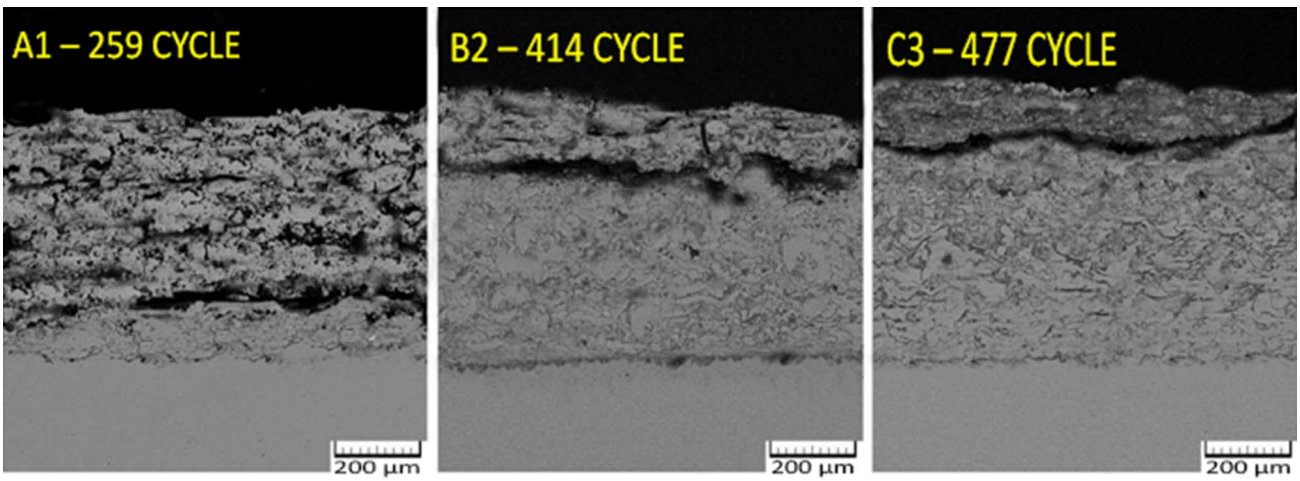

Fig. 7 Cross-sectioned micrographs of sample A1, B2 and C3 after applying thermal shock cycles

In other researches similar to this study, the same results were mentioned. For example, in study [12], to compare the thermal shock behavior of a common two-layer TBC and a nano-structured FG-TBC, a thermal shock test was done by keeping the sample at 950 °C for 5 min and quenching them in water. The obtained results were shown that the lifetime of the nano-structured coating was approximately 1.6 times more than the common coating. In addition, in research [20], thermal shock resistance was evaluated for a common TBC and a nano-structured FG-TBC. The samples were investigated in a thermal shock test by keeping them at 1020 °C and quenching in water. Its results mentioned that the thermal shock resistance of the nano-structured TBC was higher than the common one.

4 Conclusions

The thermal shock lifetime of the five-layered FG-TBC was approximately 1.6 times higher than the two-layer TBC. The observed increment in the lifetime confirmed that the creation of FGM structure in TBC enhanced quality and lifetime of the coating. Moreover, the developing top nano-structured ceramic layer was increased around 14% of the thermal shock lifetime of the films. Enhancements indicated that creating top nano-structured ceramic layer improved the quality and lifetime of the coating.

Compliance with ethical standards

Conflict of interest The authors declare that they have no known conflicts of interest.

References

1. Espanani R, Ebrahimi SH (2013) Efficiency improvement methods of gas turbine. Energy Environ Eng 1(2):36–54
2. Kokini K, Banerjee A, Taylor TA (2002) Thermal fracture of interfaces in precracked thermal barrier coatings. Mater Sci Eng A 323:70
3. Ramakrishnan S, Edwards CF (2014) Maximum-efficiency architectures for steady-flow combustion engines, II: work-regenerative gas turbine engines. Energy 72(C):58–68
4. Petrakopoulou F, Sánchez-Delgado S, Marugán-Cruz C, Santana D (2017) Improving the efficiency of gas turbine systems with volumetric solar receivers. Energy Convers Manag 149:579–592
5. Xie ZM, Liu R (2016) High thermal shock resistance of the hot rolled and swaged bulk W–ZrC alloys. J Nucl Mater 469:209–216
6. Marple BR, Lima RS, Moreau C, Kruger SE, Xie L, Dorfman M (2007) In: Marple BR, Hyland MM, Lau Y-C, Li C-J, Lima RS, Montavon G (eds) Processing and properties of yttria-stabilized zirconia TBCs produced using nitrogen as primary plasma gas, thermal spray 2007: global coating solutions. ASM International, Materials Park, pp 405–410
7. Xiaofeng W, Jiang C, Song F (2015) Size effect of thermal shock crack patterns in ceramics and numerical predictions. J Eur Ceram Soc 35:1263–1271
8. Wang Y, Bai Y, Liu K (2016) Microstructural evolution of plasma sprayed submicron-/nano-zirconia-based thermal barrier coatings. Appl Surf Sci 363:101–112
9. Guo H, Kuroda S, Murakami H (2006) Microstructures and properties of plasma-sprayed segmented thermal barrier coatings. J Am Ceram Soc 89(4):1432–1439
10. Daroonparvar M, Yajid MAM, Yusof NM (2014) Effect of Y_2O_3 stabilized ZrO_2 coating with tri-model structure on bi-layered thermally grown oxide evolution in nano thermal barrier coating systems at elevated temperatures. J Rare Earths 32(1):57–77
11. Cernuschi F, Lorenzoni L, Ahmaniemi S, Vouristo P, Mantyla T (2005) Studies of the sintering kinetics of thick thermal barrier coatings by thermal diffusivity measurements. J Eur Ceram Soc 25:393–400
12. Jamali H, Mozafarinia R, Shoja-Razavi R, Ahmadi- Pidani R (2012) Comparison of thermal shock resistances of plasma-sprayed nanostructured and conventional yttria stabilized zirconia thermal barrier coatings. Ceram Int 38:6705
13. Fan W, Bai Y (2016) Review of suspension and solution precursor plasma sprayed thermal barrier coatings. Ceram Int 42:14299–14312
14. Han Z, Xu B, Wang H, Zhou S (2007) A comparison of thermal shock behavior between currently plasma spray and supersonic plasma spray CeO_2–Y_2O_3–ZrO_2 graded thermal barrier coatings. Surf Coat Technol 201:5253
15. Su L, Chen X (2015) Numerical analysis of CMAS penetration induced interfacial delamination of transversely isotropic ceramic coat in thermal barrier coating system. Surf Coat Technol 280:100–109
16. Sun L, Tian Z (2015) Low thermal conductivity of $Lu_4Si_2O_7N_2$: theoretical and experimental studies. J Eur Ceram Soc 35:3237–3247
17. Smialek JL, Harder BJ, Garg A (2016) Oxidative durability of TBCs on Ti_2AlC MAX phase substrates. Surf Coat Technol 285:77–86
18. Joo JH, Jeong J (2014) Mosaic-shaped cathode for highly durable solid oxide fuel cell under thermal stress. J Power Sources 247:534–538
19. Gok MG, Goller G (2015) Microstructural evaluation of laser remelted gadolinium zirconate thermal barrier coatings. Surf Coat Technol 276:202–209
20. Di Girolamo G, Marra F, Blasi C, Serra E, Valente T (2011) Microstructure, mechanical properties and thermal shock resistance of plasma sprayed nanostructured zirconia coatings. Ceram Int 37:2711
21. Samal PK, Newkirk JW (2015) Powder metallurgy methods and applications. ASM handbook of powder metallurgy. 7. ISBN: 978-1-62708-089-3
22. Zhou X, Xu Z, Mu R (2014) Thermal barrier coatings with a double-layer bond coat on Ni_3Al based single-crystal superalloy. J Alloys Compd 591:41–51
23. Sharma SP, Dwivedi DK, Jain PK (2009) Effect of CeO_2 addition on the microstructure, hardness and abrasive wear behavior of flame sprayed Ni based coatings. Proc Inst Mech Eng Part J J Eng Tribol 267:853–859
24. Krishnarao RV, Alam Z, Das DK, Bhanu Prasad VV, Madhusudan Reddy G (2015) Pressureless sintering of (ZrB2–SiC–B4C) composites with ($Y_2O_3 + Al_2O_3$) additions. Int J Refract Met Hard Mater 52:55–65
25. Wu HX, Ma Z (2016) Thermal cycling behavior and bonding strength of single-ceramic-layer $Sm_2Zr_2O_7$ and

double-ceramic-layer $Sm_2Zr_2O_{7/8}$YSZ thermal barrier coatings deposited by atmospheric plasma spraying. Ceram Int 42:12922–12927
26. Han YJ, Ye FX (2014) Residual stress evolution of thermally grown oxide in thermal barrier coatings deposited onto nickel-base superalloy and iron-base alloy with thermal exposure ageing. J Alloys Compd 584:19–27
27. Soleimanipour Z, Baghshahi S, Shoja-Razavi R (2017) Improving the thermal shock resistance of thermal barrier coatings through formation of an in situ YSZ/Al_2O_3 composite via laser cladding. J Mater Eng Perform 26:1817–1824
28. Bose S (2017) High temperature coatings, Butterworth–Heinemann, eBook ISBN 9780128047439.2017
29. Wang L, Wang Y, Sun X, He J, Pan Z, Wang C (2012) Thermal shock behavior of 8YSZ and double-ceramic-layer $La_2Zr_2O_{7/8}$YSZ thermal barrier coatings fabricated by atmospheric plasma spraying. Ceram Int 38:3595–3606
30. Song S, Xiao P (2003) An impedance spectroscopy study of high-temperature oxidation of thermal barrier coatings. Mater Sci Eng 97:46
31. Zhou C, Wang N, Xu H (2007) Comparison of thermal cycling behavior of plasma-sprayed nanostructured and traditional thermal barrier coatings. Mater Sci Eng A 452:569
32. Chen X, Gu L, Zou B, Wang Y, Cao X (2012) New functionally graded thermal barrier coating system based on $LaMgAl_{11}O_{19}$/YSZ prepared by air plasma spraying. Surf Coat Technol 206:2265
33. Lima RS, Marple BR (2008) Nanostructured YSZ thermal barrier coatings engineered to counteract sintering effects. Mater Sci Eng A 485:182